JACS
JOURNAL OF THE AMERICAN CHEMICAL SOCIETY

pubs.acs.org/JACS Article

Theoretical Assessment of the Mechanism and Active Sites in Alkene Dimerization on Ni Monomers Grafted onto Aluminosilicates: $(Ni-OH)^+$ Centers and C−C Coupling Mediated by Lewis Acid−Base Pairs

Nicholas R. Jaegers and Enrique Iglesia*

Cite This: *J. Am. Chem. Soc.* 2023, 145, 6349−6361 Read Online

ACCESS | Metrics & More | Article Recommendations | Supporting Information

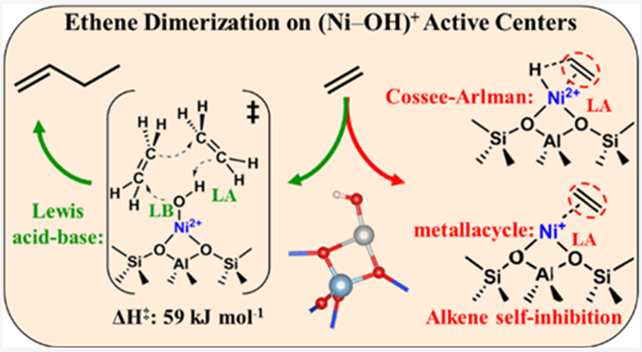

ABSTRACT: Ni-based solids are effective catalysts for alkene dimerization, but the nature of active centers and identity and kinetic relevance of bound species and elementary reactions remain speculative and based on organometallic chemistry. Ni centers grafted onto ordered MCM-41 mesopores lead to well-defined monomers that are rendered stable by the presence of an intrapore nonpolar liquid, thus enabling accurate experimental inquiries and indirect evidence for grafted $(Ni-OH)^+$ monomers. Density functional theory (DFT) treatments presented here confirm the plausible involvement of pathways and active centers not previously considered as mediators of high turnover rates for C_2-C_4 alkenes at cryogenic temperatures. $(Ni-OH)^+$ species act as Lewis acid−base pairs that stabilize C−C coupling transition states by polarizing two alkenes in opposite directions via concerted interactions with the O and H atoms in these pairs. DFT-derived activation barriers for ethene dimerization (59 kJ mol^{-1}) are similar to measured values (46 ± 5 kJ mol^{-1}) and the weak binding of ethene on $(Ni-OH)^+$ is consistent with kinetic trends that require sites to remain essentially bare at subambient temperatures and high alkene pressures (1−15 bar). DFT treatments of classical metallacycle and Cossee−Arlman dimerization routes (Ni^+ and $Ni^{2+}-H$ grafted onto Al-MCM-41, respectively) show that such sites bind ethene strongly and lead to saturation coverages, in contradiction with observed kinetic trends. These C−C coupling routes at acid−base pairs in $(Ni-OH)^+$ differ from molecular catalysts in (i) the type of elementary steps; (ii) the nature of active centers; and (iii) their catalytic competence at subambient temperatures without requiring co-catalysts or activators.

1. INTRODUCTION

C−C bond formation reactions in alkene oligomerization represent ubiquitous practical routes to increase the molecular weight of chemical intermediates. Ethene is a particularly attractive reactant because of its role as a polymer precursor and its emergence as a cost-advantaged reactant derived from shale gas resources, which has led, in turn, to shortfalls of propene and butene. Ethene dimerization on organometallic complexes proceeds via Cossee−Arlman[1] or metallacycle mechanisms,[2] but the structural complexity and architectural diversity of solid catalysts have impeded precise mechanistic descriptions and rigorous connections to mechanisms that are broadly accepted in the case of molecular catalysts.[3] Heterogeneous catalysts, with the exception of metal−organic frameworks,[4,5] do not require co-catalysts or activators, in contrast to their organometallic counterparts.[6] Ni-based solid catalysts are particularly effective for ethene oligomerization, but mechanistic details have remained notional and, in most cases, underpinned by analogies with organometallic analogues, in spite of the contrasting co-catalysts, activators, and temperatures required for these two catalyst systems.[7]

The speculative nature of such mechanistic proposals reflects, at least in part, inherent uncertainties about the identity of active Ni-based sites in solids, a persistent subject of scrutiny and contention.[8,9] Ni species based on Ni^0, Ni^+, Ni^{2+}, and Ni-alkyl species[10−14] have all been suggested as active centers for alkene oligomerization on solid catalysts, often based on sparse direct evidence.[6] Mobile Ni^{2+} complexes, rendered stable by alkyl ligands and voids of molecular dimensions, have also been proposed in the case of Ni-zeolite catalysts.[15] In many instances, the diverse and uncertain nature

Received: December 18, 2022
Published: March 13, 2023

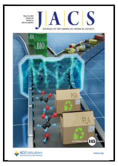

ACS Publications

https://doi.org/10.1021/jacs.2c13487

of active Ni moieties has combined with ubiquitous fast deactivation and extensive secondary C−C coupling reactions to preclude precise mechanistic inferences from the observed kinetic trends with changes in alkene pressures and reaction temperatures.

The grafting of Ni^{2+} moieties at different surface densities onto mesoporous aluminosilicates (Al-MCM-41), taken together with the discovery that the presence of a nonpolar liquid phase (alkenes or alkanes) within mesopores leads to remarkable stability during ethene, propene, and butene dimerization reactions, has allowed more accurate rate and selectivity measurements on catalysts with well-defined architectures and with unprecedented reactivity at very low temperatures (∼250 K).[16,17] These effects of nonpolar liquids reflect the preferential stabilization of dimer desorption transition states (TS) over those for the kinetically relevant C−C coupling step, thus favoring desorption over the sequential growth steps that form larger oligomers and strongly bound reaction-derived organic residues. Dimerization rates show a second-order dependence on alkene pressures, consistent with the bimolecular TS involved in C−C coupling steps and indicative of Ni-based sites that remain essentially bare of alkene-derived species, even at the very low temperatures (243−253 K) and high ethene pressures (0.1−25 bar) of these studies. Dimerization rates (per Ni atom in each sample) remained constant up to Ni contents corresponding to one Ni atom per H^+ grafting site in Al-MCM-41 supports and then decreased sharply at higher Ni contents; such observations indicate that one Ni^{2+}-containing moiety replaces a H^+ and that additional Ni atoms form structures that do not contribute to measured rates. $(Ni-OH)^+$ moieties represent the only active structure consistent with all experimental observations.[16,17] As we show here, they act as Lewis acid−base (LA−LB) pairs in stabilizing the C−C coupling TS structures, via interactions and mechanisms not previously considered for these C−C coupling reactions.

This study provides theoretical evidence for the kinetic relevance of the C−C coupling step and for the unique ability of $(Ni-OH)^+$ to interact in a concerted manner with two ethene molecules, one bound at the O atom (acting as the LB) and one at the H atom (acting as the LA) at the C−C coupling TS. Density functional theory (DFT) methods and accepted structural models for MCM-41 solids are used to assess the enthalpy and free energy of relevant bound species and TS structures for ethene reactants, but the conclusions remain relevant for higher alkenes, which show similar experimental kinetic trends and effects of Ni content and intrapore liquids on dimerization rates.[17] These theoretical methods also show that alkene dimerization does not proceed via routes mediated by carbenium ions (as in C−C coupling on Brønsted acids) or on active sites consisting of Ni^+ (metallacycle routes)[2] or $Ni^{2+}-H^-$ (Cossee−Arlman routes),[1] which would bind ethene very strongly, in contradiction to the measured effects of ethene pressure on dimerization rates. We surmise that moieties resembling the $(Ni-OH)^+$ considered here and containing LA−LB pairs may form, at least in some cases, through the use of additives required for reactivity with organometallic and metal−organic framework catalysts, thus accounting for the role of activators and co-catalysts in such cases.

2. COMPUTATIONAL METHODS

Periodic DFT calculations were carried out with the Vienna Ab initio Simulation Package (VASP; version 5.4.4[18]) on the XSEDE platform.[19] Interactions between core and valence electrons were described using projector-augmented wave pseudopotentials.[20] Plane-wave basis sets were cut off at 450 eV for all calculations. Cutoff energies above 450 eV resulted in electronic energy changes smaller than 0.02% (Figure S1, Supporting Information (SI)). Exchange and correlation were treated using the generalized gradient approximation as prescribed by Perdew−Burke−Ernzerhof methods.[21] The modified dispersion correction by Grimme et al. combined with Becke−Johnson damping (D3-BJ) was used to account for long-range dispersion-type interactions.[22] A Monkhorst−Pack[23] *k*-point 1 × 1 × 1 grid was used to sample the Brillouin zone; this lessened computational expense without a loss of accuracy, as evidenced by energies that differed by less than 0.5 kJ mol^{-1} from those on 3 × 3 × 1 sampling grids; electronic structures were converged to 10^{-6} eV in self-consistent steps, previously shown to be an appropriate convergence criterion for the Al-MCM-41 model.[24] The expected presence of unpaired d-orbital electrons in Ni^{2+} required that all calculations be conducted in spin-unrestricted mode.

Geometries were optimized with a force-based convergence criterion of 0.5 eV nm^{-1}. Multiple geometric configurations (e.g., at least three different binding orientations or distances, the sequence of ethene adsorption at either the O atom or the H atom) were examined, and the most stable configurations are reported here. Transition state (TS) structures were isolated using the nudged elastic band (NEB) approach.[25] The results of the NEB computation were first refined using the Climbing Image method[26,27] to more accurately determine the saddle point and then optimized using the Henkelman dimer method.[28] Converged TS structures were confirmed by the existence of a single imaginary frequency. Vibrational frequencies for surface and gaseous species were calculated using the second derivative of the energies with respect to atomic positions by perturbing each atom by ±0.001 nm. Enthalpies, entropies, and Gibbs free energies were computed using the DFT results and statistical mechanics formalisms by referencing the relevant energy of the structure to that of a bare surface and gas-phase ethene.[29] Since the vibrational analysis approach uses harmonic oscillator formalisms that often fail to accurately describe low frequencies modes,[30] resulting in severe overestimations of the entropy of adsorbates, contributions from low-frequency modes (<100 cm^{-1}) were replaced with a fraction (0.7) of the rotational and translational entropy and enthalpy of the gaseous analogue of the surface species at 1 bar.[31−33] A comparison of the contributions from rotational, translational, and vibrational entropies using statistical thermodynamics with reference values of entropies for gas-phase ethene[34] confirmed excellent agreement between the computational−statistical approach with experiments (219.0 vs 219.5 J mol^{-1} K^{-1}).

Enthalpies (H) were determined by

$$H = E_0 + E_{ZPV} + H_{vib} + H_{trans} + H_{rot} \quad (1)$$

Here, E_0 is the DFT-derived electronic energy, E_{ZPV} is the zero-point vibrational energy, and the H terms reflect the vibrational, translational, and rotational contributions of enthalpy. Entropies (*S*) were similarly composed of the relevant vibrational, translational, and rotational components. A more complete description of the free energy computation from statistical thermodynamics treatments[35] is available in eqs S1−S11 in the SI. All reported enthalpies, free energies, and entropies are reported for 243 K, unless otherwise noted.

Aluminosilicate slabs were constructed using methods reported for MCM-41 silica surfaces.[36] A four-layer silicate slab of 1.2 nm thickness and 1.3 × 1.3 nm width ($Si_{60}O_{124}H_8$ per unit cell) was extracted from a channel wall of Si MCM-41 models; such slabs were large enough to prevent repulsive lateral interactions among reactants in vicinal cells.[24] Periodic images were separated by 4 nm vacuum layers in the *z*-direction; dipole and quadrupole moments were calculated parallel to the *z*-lattice vector to correct the total energy for interactions among periodic slabs.[24,37,38] The aluminosilicate form of these models was constructed by replacing a surface Si atom with Al atom at the location that minimized the electronic energy of the system and adding a proton at an adjacent O atom so as to maintain charge neutrality. Site models for Ni species requiring one framework oxygen anchoring site (e.g., $(Ni{-}OH)^+$) were constructed by replacing the charge-balancing H atom (Brønsted acid site) by the Ni atom in the Ni species of interest and optimizing the structure geometry. Models consisting of Ni^{2+} species require two framework grafting sites and were generated by replacing the proximal surface Si atom with an Al atom so as to give the lowest energy, substituting both charge-balancing protons with Ni^{2+}, species and optimizing the geometry. All bare Ni site models were structurally relaxed and subsequent computations including hydrocarbons used fixed atomic positions for bulk Si and O atoms in Al-MCM-41 farther than five bonds away from the Ni species (160 atoms) to save computational resources and ensure that computed energetics solely reflect binding and reactivity on the Ni centers.

Dipole and quadrupole energy corrections are inaccurate for charged slab models.[39] As a result, OH-terminated cluster models of the aluminosilicate and $(Ni{-}OH)^+$ site ($Si_{47}AlO_{122}H_{53}$ and $Si_{47}AlO_{123}H_{53}Ni$) were extracted from the slab model described above to estimate deprotonation energies (DPE), a rigorous measure of the proton-donating ability of Brønsted acids and thus of their acid strength.[40] DPE values (eq 2) represent the energy required to separate a proton (H^+) from the conjugate anion (e.g., AlO^-) to noninteracting distances

$$\mathrm{DPE} = E_{\mathrm{H}^+} + E_{\mathrm{Z}^-} - E_{\mathrm{HZ}} \tag{2}$$

where E_{Z^-}, E_{H^+}, and E_{HZ} are the energies of anionic cluster, gaseous H^+, and neutral cluster, respectively. DPE values have been extensively used as a descriptor of acid strength for solid acids and serve as a metric for predicting the reactivity of Brønsted acids in acid-catalyzed reactions.[40−42]

The coverages of bound species at $(Ni{-}OH)^+$, Ni^+, $Ni^{2+}{-}H^-$, and Ni^{2+} were each obtained using Langmuirian adsorption models (eq 3)

$$\theta_{C_2H_4} = \frac{K_{eq}P_{C_2H_4}}{1 + K_{eq}P_{C_2H_4}} \tag{3}$$

where θ is the fractional site coverage by ethene, K_{eq} is its equilibrium constant, and P is the contacting ethene pressure. Adsorption constants were estimated from the DFT-derived free energies of formation of bound species from their gaseous counterpart at each type of binding site.

3. RESULTS AND DISCUSSION

3.1. Evidence for the Presence and Catalytic Involvement of $(Ni{-}OH)^+$ Species.

The grafting of Ni^{2+} species by replacing H^+ in aluminosilicates can form Ni monomers and oligomers, which can act, in turn, as potential active centers for alkene dimerization turnovers; these species may reduce during reaction (or activation) to form Ni^+ or $(Ni^{2+}{-}H^-)$ species. Infrared spectra of bound CO detected several types of Ni species grafted at various exchange locations (silanol nests, extra-framework Al), as well as NiO domains, in a given Ni/BEA sample, an indication of the challenges inherent in establishing their respective contributions to dimerization turnovers.[43,44] Single-site structures were reported using low Ni contents and grafting from hexamine complexes onto Al-BEA zeolites (Si/Al = 12) so as to garner mechanistic insights from spectroscopic investigation, but kinetic assessments of reaction rates were not feasible because of very rapid deactivation caused by the formation of large oligomers.[45] In contrast, a systematic examination of samples prepared by contacting aqueous Ni^{2+} species with mesoporous Al-MCM-41 to give 0.1−8.0 Ni^{2+} per (original) H^+ in the parent Al-MCM-41 showed that dimerization rates (per mass) for ethene, propene, and butene increased linearly with Ni content up to a Ni^{2+}:H^+ exchange stoichiometry of unity and then remained constant at higher Ni contents.[16,17] Such catalytic consequences of exchange stoichiometry indicate that each active Ni^{2+} species replaces one H^+, thus ruling out Ni^{2+}, $Ni^{2+}{-}O{-}Ni^{2+}$, or $Ni^{3+}{-}H$ species as active centers because such species would require two (vicinal) grafting sites; such vicinal sites are not likely to prevail at the low H^+ areal densities (0.1 H^+ nm^{-2}) and high Si/Al ratio (40) in these Al-MCM-41 supports.[16,17] These observations reflect instead the predominant presence of monomeric Ni species. As shown in Section 3.4, Ni^+ and $Ni^{2+}{-}H$ reflect reaction intermediate coverages which are inconsistent with experimental observations, thus implicating the presence of $(Ni{-}OH)^+$ species and their exclusive catalytic involvement and the formation of unreactive NiO domains at exchange stoichiometries above unity.

Mean Al−Al distances in the Al-MCM-41 sample used (0.1 H^+ nm^{-2}) are 3.6 nm, a scale that cannot accommodate vicinal grafting sites unless Al pairing is favored by energy considerations. A preference for such pairing is examined here by extracting a periodic unit containing 142 Si atoms from the MCM-41 structure and replacing one Si with an Al at the location giving the minimum energy. This substitution was then repeated at locations differing in distance from the Al atom initially placed. The energies of the slab with the two Al atoms (Figure S2) did not show any discernible preference for Al pairing in the MCM-41 framework or any evident trends in electronic energies with Al−Al distance for a series of Al substitution combinations (1.256−1.287 eV for 0.4−0.5 nm distance and 1.257−1.274 eV for a 1.5−2.1 nm distance). The high Si/Al ratio (40) in the samples used to derive these inferences about mechanisms and site requirements, as well as the absence of synthetic attempts at Al pairing in these samples through the use of structure-directing templates[46] or alkaline earth cations[47] that encourage Al−Al pairs, make it unlikely that such pairs exist to act as grafting points for Ni^{2+} cations; such species, in any case, would lead to the titration of all grafting sites at 0.5 Ni^{2+} per H^+, in contradiction with experimental observations.

Alkene dimerization rates (per Ni) that remain constant up to a grafting stoichiometry of unity and decrease thereafter (thus leading to constant mass-normalized rates) indicate that NiO domains are not responsible for catalysis and that they merely act as unreactive spectators after grafting sites are depleted by exchange. Moreover, chemical reduction treatments (H_2; 673 K) did not improve measured dimerization rates,[48] indicating that active Ni species are either generated directly through the synthetic protocols used or formed rapidly upon contact with alkene reactants. The titration of sites by 2,6-di-*tert*-butylpyridine (DTBP; to a DTBP/Ni stoichiometry of unity) during catalysis implicates the involvement of $(OH)^-$ groups on grafted Ni centers for dimerization reactions. Similarly, titration of the Lewis acid centers by CO fully suppressed dimerization rates, demonstrating the concerted nature of both the acid and base functions in dimerization catalysis.[17] These observations provide compelling evidence for $(Ni{-}OH)^+$ monomers as the active centers that are responsible for the unprecedented reactivity of these materials at subambient temperatures.

Such conclusions deserve theoretical confirmation because such sites and associated mechanisms have not been

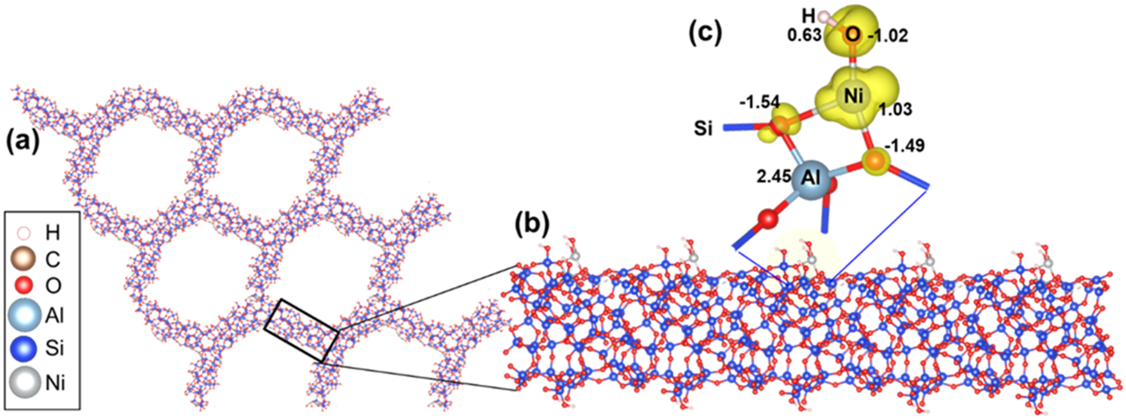

Figure 1. (a) Model structure for Al-MCM-41 with the segment extracted from the unit cell highlighted. (b) Extracted periodic slab with the (Ni−OH)$^+$ site deposited at the Al-exchange position. (c) Unpaired electron density (yellow) and Bader charges for the local structure around Ni.

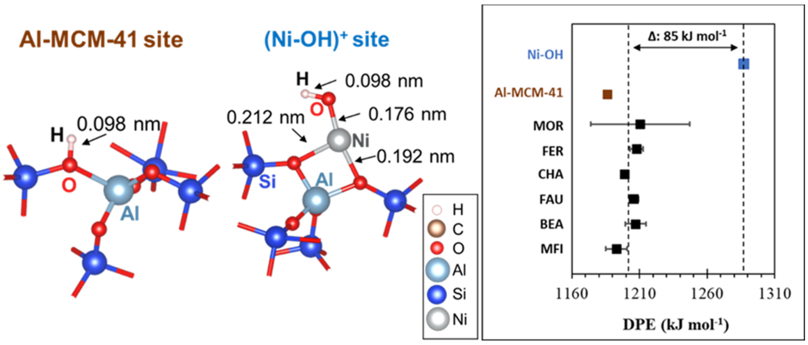

Figure 2. DFT-derived structures of the Al-MCM-41 H$^+$ site and the (Ni−OH)$^+$ site and calculated deprotonation energies for the two species plotted with DPEs extracted from the literature.[40] The range bars on DPE points for zeolite frameworks indicate the range among all crystallographically distinct H$^+$ locations in the framework.

considered, even after several decades of exhaustive examination of Ni-catalyzed oligomerization reactions, whether on solids or organometallic systems.[10,14,49,50] These theoretical assessments involve the substitution of an Al atom for a Si atom in the MCM-41 model structure depicted in Figure 1a and the compensation of the aluminosilicate framework charge with a H$^+$ at an O$^-$ site adjacent to Al. A slab model was extracted from such mesoporous structures, and (Ni−OH)$^+$ moieties were used to replace each H$^+$ site (Figure 1b) and used in all calculations involving (Ni−OH)$^+$ species. The electronic structures of these (Ni−OH)$^+$ species were also probed by calculating the density of unpaired spins (using spin-polarized calculations) for Ni atoms with a [Ar]3d^{8}4s^2 ground state and unpaired electrons in the $d_{x^2-y^2}$ and d_{z^2} orbitals, and from a Bader charge analysis (Figure 1c); these calculations show that the unpaired electrons are localized around the Ni atom. The Bader charge analysis indicates that a cationic Ni species has replaced the H$^+$ species as charge-balancing species, shown by a total computed charge of (Ni−OH)$^+$ is 0.64. (Ni−OH)$^+$ is thus considered as a plausible species that can form through the grafting protocols used to prepare these samples.

3.2. Identity and Kinetic Relevance of Elementary Steps and Bound Intermediates in Ethene Dimerization on Grafted (Ni−OH)$^+$ Centers.

Alkene oligomerization reactions can occur on solid acid catalysts via proton transfer routes mediated by carbenium ion transition states.[51−55] Such mechanisms involve the transfer of the proton in the solid acid to an incipiently formed dimer at the kinetically relevant bimolecular TS, with the formation of an alkoxide as alkene reactants bind in the immediately preceding step. Both steps require the deprotonation of the acid in the formation of the relevant TS structures for both alkoxide formation and C−C coupling steps. In the former step, one sp^2 hybridized C atom in the alkene accepts the H$^+$ and the other sp^2 hybridized carbon binds to the conjugate anion to form a covalently bonded alkoxide.

The H$^+$ species in Al-MCM-41 (without grafted Ni^{2+}) indeed showed ethene dimerization reactivity, but at rates (per mass) about 10^3-fold lower than after Ni^{2+} grafting (12 bar and 248−503 K).[16,17] The free energy of formation of the requisite carbenium ion TS for these reactions on Brønsted acids depends on the DPE of the solid acid, leading to dimerization rates that increase exponentially as DPE decreases.[56] Any contributions from proton transfer to bound intermediates from (Ni−OH)$^+$ sites would require that DPE values for (Ni−OH)$^+$ be significantly smaller than for aluminosilicates; the latter solid acids exhibit DPE values that depend only weakly on their framework structure, either as mesoporous amorphous forms or as microporous crystalline solids, such as zeolites.[40]

DFT-derived DPE values for the OH groups in Al-MCM-41 and in (Ni−OH)$^+$ species show that carbenium ion pathways would be much less competent on the latter species than on Al-MCM-41, rendering such routes undetectable on samples with grafted Ni centers. Figure 2 depicts the structure and bond length of the OH groups that act as the Brønsted acid in (Ni−OH)$^+$ and aluminosilicate acids. The O−H bond lengths in (OAlO−H)$^+$ and (NiO−H)$^+$ species are similar (0.098 nm)

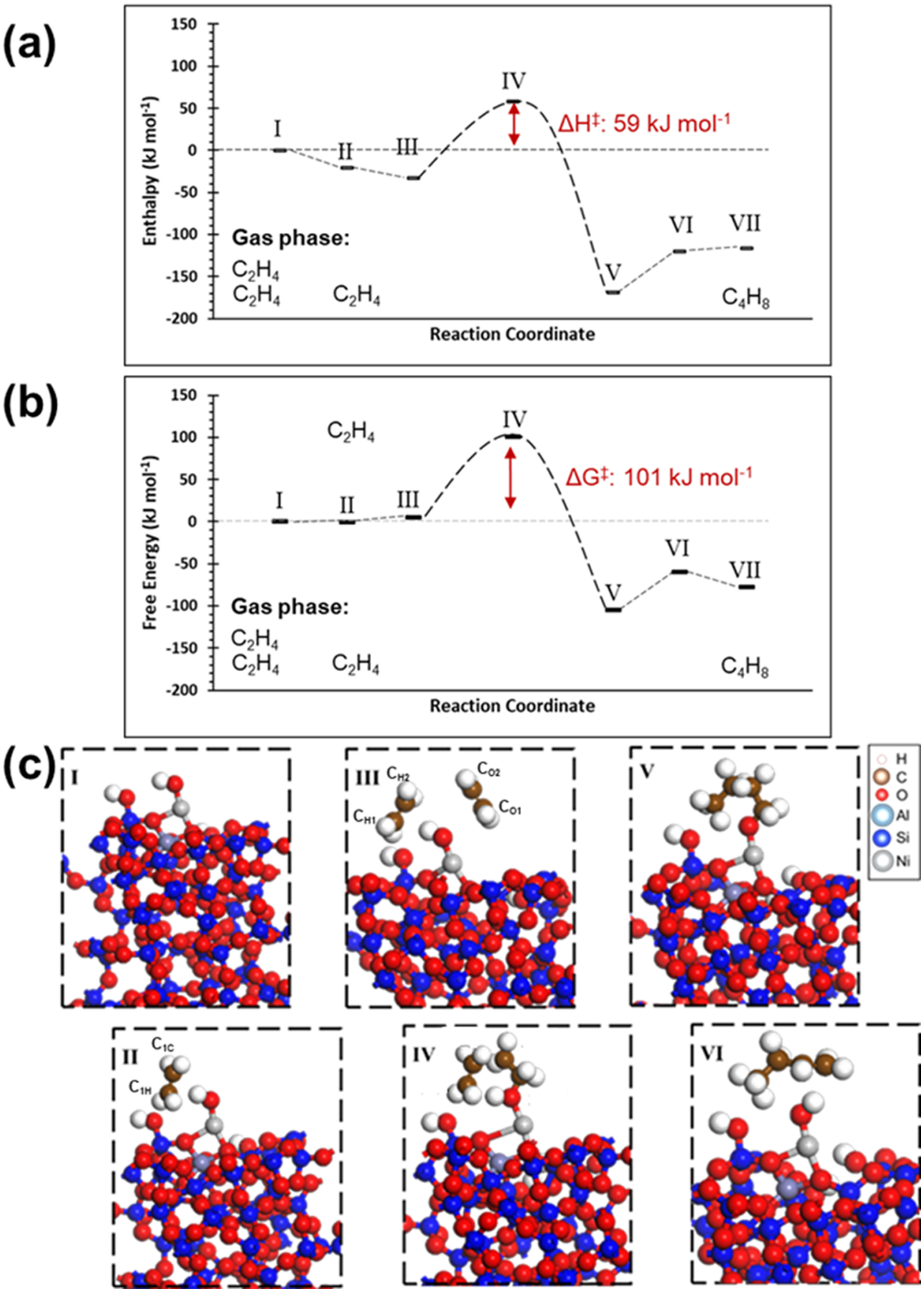

Figure 3. Reaction coordinate diagram of DFT-assessed ethene dimerization via a concerted acid−base mechanism over model (Ni−OH)$^+$ sites. Energies are reported with respect to a bare (Ni−OH)$^+$ site and two gas-phase ethene molecules at 1 bar, 243 K. (a) Enthalpies reflect corrected electronic energies for zero-point vibrational energy and (b) free energies assume 0.7 of the gas-phase rotational and translational entropy (see the Computational Methods sections and the SI). (c) DFT-optimized geometries are shown for each species with ethene carbon labeling reflecting the ethene interactions with H or O in (Ni−OH)$^+$ and if the atom is relatively nearer or farther from the surface (1 and 2, respectively).

and typical of O−H groups in aluminosilicate Brønsted acids (0.0974−0.1009 nm).[40,57] As shown previously, there are no discernible correlations between O−H bond lengths and DPE values.[40] DFT-derived DPE values merely reflect the stability of the structure that remains after deprotonation (the conjugate anion). These DPE values are 1287 kJ mol^{-1} for (Ni−OH)$^+$ and 1186 kJ mol^{-1} for (OAl−OH)$^+$ in Al-MCM-41 (Figure 2), a large difference that shows that (Ni−OH)$^+$ is a much weaker acid than aluminosilicates and would yield much smaller dimerization turnover rates than Al-MCM-41; in contrast, experimental observations show much higher turnover rates on Ni-containing Al-MCM-41 samples, in which the H$^+$ centers in Al-MCM-41 have been titrated by grafted Ni^{2+} species.[16] Figure 2 also shows DPE values reported previously for zeotypes and corrected for artifacts imposed by periodic DFT methods (1193−1210 kJ mol^{-1}, averaged over all crystallographically distinct (OAl−OH)$^+$ locations in MFI and MOR frameworks).[40] Computations for the acidic Al-MCM-41 site are consistent with those of other aluminosilicates and their generally weaker Brønsted acid strength relative to polyoxometalates and super acids (1100 kJ mol^{-1}).[58]

3.3. Ethene Dimerization Routes Are Mediated by Concerted Interactions with Lewis Acid−Base Pairs at C−C Coupling Transition States. Kinetic trends with changes in alkene pressures indicate that C−C coupling elementary steps are kinetically relevant and occur at Ni centers that are sparsely covered by alkene-derived species (for ethene,[16] propene, and butene[17]). Dimerization rates were weakly influenced by the presence of intrapore nonpolar liquids, indicative of predominant TS stabilization through interactions with the Ni-based active centers (only selectivity and stability were strongly influenced by a liquid phase),[16,17] thus enabling comparisons of reactivity between experiments and theory without the use of theoretical treatments that include solvation by liquids. The previous section demonstrated that well-established pathways involving proton transfer and carbenium ions cannot occur at detectable rates on $(Ni-OH)^+$ sites and thus are unable to account for the very large rate enhancements observed when protons are replaced by $(Ni-OH)^+$. This section specifically addresses how $(Ni-OH)^+$ centers are able to interact with ethene molecules in a manner that stabilizes the C−C coupling TS so as to lead to very fast dimerization turnovers at subambient temperatures (∼250 K).

Such alternate routes must avoid cationic $C_2H_5^+$ species and allow $(Ni-OH)^+$ species to align (structurally and electronically) the two ethene molecules required to form a C−C bond, through electron rearrangements that enable concerted interactions with the H, O, or Ni atoms in $(Ni-OH)^+$ centers; in doing so, some of these atoms act as Lewis acids (H^+, Ni^{2+}) and others as Lewis bases (O anions). These reaction channels are explored here on the $(Ni-OH)^+$ and MCM-41 model structures described above using ethene as the illustrative alkene reactant.

The DFT-derived enthalpies and free energies of ethene molecules reacting on $(Ni-OH)^+$ centers (at 243 K) are depicted in Figure 3 in the form of a reaction coordinate diagram. The computed enthalpy and Gibbs free energy for the formation of 1-butene from two ethene molecules in the gas phase are −115.9 and −77.4 kJ mol^{-1} (Table 1), in good agreement with thermochemical data[34] at 243 K (−106 and −72.1 kJ mol^{-1}, respectively). Such agreement indicates that DFT-derived energies, zero-point vibrational corrections, and statistical mechanics formalisms are able to describe the relevant thermodynamic properties of gaseous ethene and 1-butene molecules.

Table 1. DFT-Derived Enthalpies and Free Energies for the Formation of Each Species in the Proposed Concerted Acid−Base-Catalyzed Ethene Dimerization Pathway on $(Ni-OH)^+$ Sites from Figure 3[a]

structure	ΔH (kJ mol^{-1})	ΔG (kJ mol^{-1})
I	reference	reference
II	−20.0	−0.5
III	−32.6	5.0
IV	58.8	100.7
V	−168.1	−104.6
VI	−119.9	−59.6
VII	−115.9	−77.4

[a] Energies are with respect to a bare $(Ni-OH)^+$ site and two gas-phase ethene molecules at 1 bar, 243 K.

Interactions between ethene and $(Ni-OH)^+$ sites lead to slightly exothermic adsorption (−20 kJ mol^{-1}, Table 1; species II), but the associated entropy losses lead to adsorption free energies that are essentially zero (−0.5 kJ mol^{-1}; 243 K). Such species involve weak interactions of the H atom in $(Ni-OH)^+$ with the ethene π-bond; an alternate mode, in which ethene interacts via the ethene H atoms with the O atom in $(Ni-OH)^+$, gave slightly less favorable adsorption enthalpies (by about 15 kJ mol^{-1}) and an adsorption free energy of +12 kJ mol^{-1}. The addition of a second gaseous ethene to species II forms species III, in which one C atom in the first ethene interacts with the H atom of $(Ni-OH)^+$ (C_{H1}) and one C atom in the second ethene interacts with the O atom in the $(Ni-OH)^+$ center (C_{O1}). The enthalpy for the conversion of species II to species III is −12 kJ mol^{-1}, but the reaction free energy is positive (+6 kJ mol^{-1}). Both ethene molecules become polarized via interactions with the Lewis acid (H atom) and base (O atom) centers in $(NiO-H)^+$. The ethene molecule at $(Ni-OH)^+$ in species II shows differences in Bader charge relative to gaseous ethene of −0.02 and +0.1 for the carbon atom of the ethene proximal to H of $(NiO-H)^+$ (C_{H1}) and the other carbon in ethene which will form a C−C bond in species IV (C_{H2}) (Figures 3 and 4), respectively; these charges are indicative of weak polarization induced by interactions with the net positive charge of the $(H-ONi)^+$ species through the H atom, which withdraws electron density from ethene. Upon adsorption of a second ethene molecule (species III) near the electron-donating O atom of $(NiO-H)^+$, the charge on C_{H1} is slightly perturbed. This second adsorbed ethene also shows charge redistribution relative to gaseous ethene with C_{O1} and C_{O2} exhibiting Bader charges of −0.06 and −0.16, respectively. Those carbon atoms most closely bonding to $(Ni-OH)^+$ (C_{H1} and C_{O2}) are polarized in opposite directions upon adsorption and closer coordination to Lewis acid H atoms and Lewis base O atoms shown in the C−C coupling transition state (species IV).

NEB and dimer methods were used to isolate the TS for the kinetically relevant C−C coupling step[14,15] involving species III. This TS (species IV) represents the highest enthalpy (and free energy) along the reaction coordinate (Figure 3); its imaginary vibrational frequency corresponds to the symmetric motion of the two nearest C atoms (C_{H2} and C_{O2}) in the two ethene molecules in species III along the axis connecting these two C atoms. The bond distance in the incipiently formed C−C bond at the TS is 0.23 nm (Figure 4) and exceeds that in the product structure (0.153 nm), but it is much shorter than in structure III (0.411 nm; the reactant state). The Ni−O bond in $(Ni-OH)^+$ at the TS is slightly elongated (0.184 nm) relative to the initial state (0.174) because of electronic interactions of bound alkenes with the H−O Lewis acid−base pair. The NiO−H bond in $(Ni-OH)^+$ is minimally perturbed (0.099 nm at the TS (IV); 0.098 nm in species I and species III) and interacts with C_{H1} in ethene at a distance of 0.2 nm. This H−C_{H1} bond length is slightly smaller than in structure III (0.22 nm), but nearly twice the length for the butoxide in species V (0.11 nm). The C−O bond between ethene and the O atom in $(Ni-OH)^+$ becomes shorter as species III (0.327 nm) forms the TS (0.145 nm) and resembles closely the C−O bond in the product state (species V; 0.141 nm). This evolution in bond lengths indicates that the TS exhibits product-like geometry, consistent with experimental measurements that reflect entropic losses more consistent with product dimers than substrate monomer alkenes and indicate a late

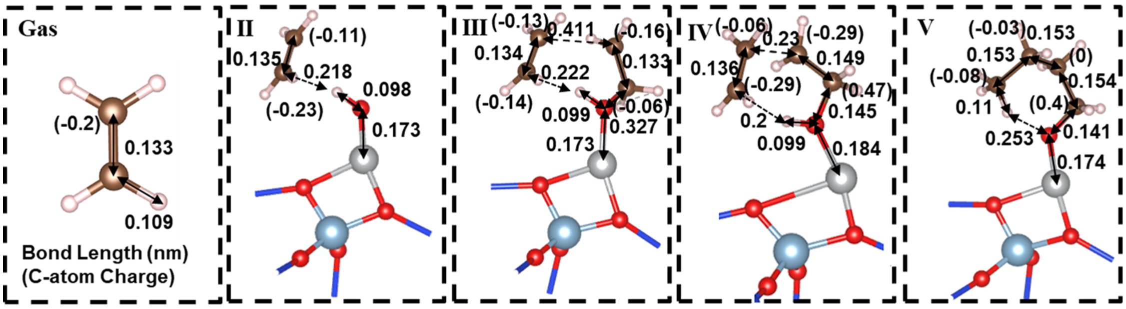

Figure 4. Bond lengths and charges for structures of DFT-assessed ethene dimerization via a concerted acid–base mechanism over model (Ni–OH)$^+$ sites. Bond lengths are reported in nm. Charges are reported in parentheses.

product-like transition state.[17] Such a late TS for an exergonic reaction is not typical or consistent with the Hammond Postulate; it suggests that the product minimum (species V) lies within a narrow potential well (large force constant for vibrational displacements) relative to the reactant (species III),[59] or that vibration modes parallel to the reaction coordinate contribute to the distribution of electron density at the TS.[60]

The enthalpy of formation of this C–C coupling TS from two gaseous ethene molecules (one bar) and (Ni–OH)$^+$ (species I) is +58.8 kJ mol^{-1} (Figure 3a and Table 1), a modest barrier that is commensurate with the remarkable competence of such active centers in catalyzing C–C coupling reactions of alkenes. This enthalpy value is also in good agreement with measured activation barriers (46 ± 5 kJ mol^{-1}),[17] especially in light of the approximate nature of the structural models used here to describe the anchoring of the (Ni–OH)$^+$ centers and the aluminosilicate substrate. Rate constants computed with respect to a pressure of 1 bar of ethene (adapted from those reported as (mol s^{-1} MPa^{-2} Ni^{-1}), shown in Figure S3),[17] and regressing activation entropies ($\Delta S^{\ddagger}$) from measured rate constant preexponential factors,[a] reveals a $\Delta S^{\ddagger}$ of −138 J mol^{-1} K^{-1} at 1 bar, which reflects the entropy of formation of the C–C coupling TS from two gaseous ethene molecules.

The ubiquitous inaccuracies in using DFT vibrational modes of surface adsorbates to estimate entropies arise from the use of harmonic oscillator approaches which have shallow potential energy wells that can deviate from intramolecular vibrational modes.[30−33] To circumvent this, an empirical approach that replaces the low-frequency modes of adsorbates with a fraction (0.7) of the gas-phase rotational and translational entropy of adsorbates (one or two ethene or one 1-butene molecule) was employed, based on heuristic arguments observations for the retention of significant fraction of the gas-phase rotational and translational motion upon adsorption to a surface.[31−33]

The resulting $\Delta S^{\ddagger}$ (Table 2) depicts estimates of activation entropies for retention of a fraction of 0.7 (−172 J mol^{-1} K^{-1}) of the gas-phase rotational and translational entropy, significantly larger than measured (−138 J mol^{-1} K^{-1}). The convention of 0.7 of the gas-phase entropy yields activation free energies of 100.7 kJ mol^{-1} (1 bar, 243 K), also notably larger than those measured (79.5 kJ mol^{-1}). These discrepancies predominantly reflect entropy estimates for the bound species, and the retention of 0.8 of the gas-phase rotational and translational entropy (−136 J mol^{-1} K^{-1}) shows consistence with measured values. This slightly larger retention of gas-phase entropy upon adsorption may reflect the less-constrained nature of the adsorbed species and a relatively higher degree of such motions allowed by surface (Ni–OH)$^+$ sites.

Table 2. Computed Activation Entropies for the C–C Coupling Transition State for Adsorbates Retaining 0.7 and 0.8 Fractions of Their Gas-Phase Rotational and Translation Entropy[a]

retention criterion	$\Delta S^{\ddagger}$ (J mol^{-1} K^{-1})
$0.7S_{gas}$	−172
$0.8S_{gas}$	−136

[a] S_{ethene} is 219 J mol^{-1} K^{-1}; of this, 195.7 J mol^{-1} K^{-1} are rotational and translational contributions.

The noted differences in computed enthalpies and free energies may also highlight the challenge and limitations of accurately assessing energetics by DFT methods, for example, the selection of the PBE-D3 functional. PBE is known to overestimate lattice dimensions of aluminosilicates, so dispersion corrections are often incorporated, which can overcorrect some systems with extensive hydrogen and π-bond interactions[61,62] or for hydrocarbon adsorptions on carbon surfaces.[63] The difference in enthalpy here, however, we regard as a reasonable approximation in support of the interpretation of experimental results.

The Bader charges at each C atom in bound ethene molecules differ from those in their gaseous form as a consequence of the polarization induced by interactions with the Lewis acid (H atom) and base (O atom) centers in (Ni–OH)$^+$. Such perturbations are most evident as the new C–C bond incipiently forms at the TS (species IV; Figures 3 and 4). At the TS, C atoms in the ethene molecule interacting with the H of (Ni–OH)$^+$ (C_{H1} and C_{H2}, Figure 3) become more polarized than in the precursor structure (species III; −0.29 and −0.06, respectively). The ethene molecule interacting with the O atom in (Ni–OH)$^+$ in species III is more strongly polarized at the TS (species IV), with C_{O1} and C_{O2} exhibiting charges of 0.47 and −0.29, respectively, compared to −0.06 and −0.16 in species III. The two ethene molecules in structure IV (Figure 3c) are polarized in opposite directions by interactions with the Lewis base O and Lewis acid H species in the Lewis acid–base (Ni–OH)$^+$ center (C_{H2} and C_{O2} have opposite charges relative to the gas-phase ethene: +0.14 and −0.09, respectively); such perturbations in electron density lead to electrostatic interactions that promote the charge transfer required to form a new C–C bond between C_{H2} and C_{O2}.

After completing C–C coupling through the TS (species IV), a butoxide is formed and is exothermic (species V; −168 kJ mol^{-1}) with respect to two gaseous ethene molecules and a bare $(Ni-OH)^+$ center. The butoxide binds through its C_{O1} to the O atom in $(Ni-OH)^+$. H transfer from the butoxide back to the Ni–O center forms a bound 1-butene (structure VI) with its π-bond interacting with the H atom in $(Ni-OH)^+$ in a manner that resembles the binding of ethene as species I. The resulting entropy gain from species V to VI (13.2 J mol^{-1} K^{-1}) favors its desorption and enthalpic effects brought forth by intrapore liquids stabilize these late desorption TS structures, thus preventing the loss of selectivity and the ultimate blocking of active centers caused by subsequent oligomerization events before desorption.[16,17]

Previous studies of ethene dimerization have reported a broad range of butene selectivities (among all products) from 20% on Ni silicates systems to 95% on Ni-MOF systems at temperatures higher than in the present study (423 K, 35 bar and 283 K, 15 bar, respectively).[64,65] Reactions on Ni–Al-MCM-41 at 243 K in the presence of intrapore liquids led to the exclusive formation of 1-butene at low conversions (<1%) and decreased dimer selectivities with increasing conversion (80% 1-butene and 97% all butenes at 10% conversion) as a result of readsorption and subsequent isomerization and chain growth of primary dimer products along the catalyst bed.[16] The absence of intrapore condensation leads to lower butene selectivities (~93% at 448 K, conversion <1%), with considerable isomerization of 1-butene.[16] Oligomerization of larger alkenes reflects product selectivities that also favor dimerization under conditions of intrapore condensation, but sequential oligomerization prevails in the absence of intrapore condensation (selectivities of 41% to hexene and 15% to octene for propene and 1-butene dimerization, respectively).[17]

The proposed ethene dimerization route is depicted as a complete catalytic cycle in Figure 5; these pathways, first proposed based on kinetic trends[16,17] and confirmed here through theoretical assessments, represent a plausible C–C coupling route on the $(Ni-OH)^+$ centers shown to act as the active sites from the effects of grafting stoichiometry on measured dimerization rates for C_2–C_4 alkenes. Experimental kinetic trends show a second-order rate dependence on alkene pressures,[16,17] consistent with a bimolecular TS for the kinetically relevant step and with the prevalence of unoccupied $(Ni-OH)^+$ sites during catalysis, even at low temperatures and high alkene pressures (0.1–15 bar, 243–448 K). DFT-derived enthalpies for ethene binding on $(Ni-OH)^+$ (species II, ΔH: −20 kJ mol^{-1}; species III, ΔH: −32.6 kJ mol^{-1}) are consistent with weak interactions of ethene with active centers. DFT-derived energies and entropies for ethene binding onto $(Ni-OH)^+$ centers determine site occupancy through Langmuirian formalisms and the free energies for the binding of one ethene (species II) and two ethene (species III) (−0.5 and +5 kJ mol^{-1}, respectively; 243 K) on $(Ni-OH)^+$; these free energies lead, in turn, to fractional site coverages of 0.56 and 0.08 (at 1 bar ethene, 243 K, Figure 6a). The coverages would have led to detectable deviations from second-order kinetic trends, but their low (but consequential) values are likely to reflect inaccuracies in structural models and DFT methods; they are consistent with weak binding of reactants at $(Ni-OH)^+$ and stand in contrast with the very strong binding of ethene at Ni^+ and $Ni^{2+}-H^-$ that is described in Section 3.4.

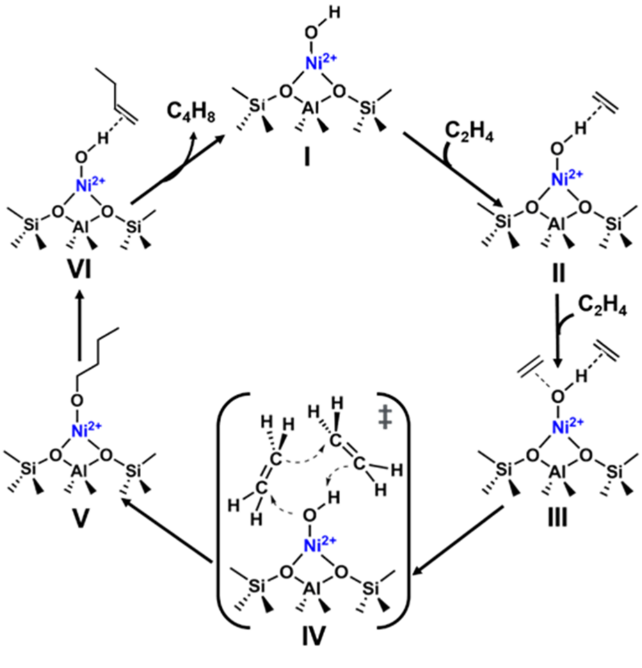

Figure 5. Probable ethene dimerization catalytic cycle on $(Ni-OH)^+$ moieties acting as a Lewis acid–base pair proposed from a DFT analysis of ethene reactions on Ni–Al-MCM-41.

The DFT-derived enthalpy of formation of bound 1-butene from two gaseous ethene molecules and a $(Ni-OH)^+$ site (species VI) is −200 kJ mol^{-1} (1 bar, 243 K). This value indicates the stronger binding of 1-butene products than ethene reactants. Though detectable coverages would be expected from such negative enthalpies, determination of these coverages should instead reflect the energy difference between the bare site and the gas-phase dimer and the adsorbed dimer on the site. This is valid for desorption steps which are stabilized by intrapore liquids to yield quasi-equilibrated desorption of dimers. With reference to a bare site and gaseous 1-butene, the enthalpy of adsorption for 1-butene is +4 kJ mol^{-1} leading to site coverages of 10^{-8}–10^{-5} (Figure 6a) for mean ethene conversions of 1 and 10% at ethene pressures of 0.1–15 bar.[16,17] Such coverages are consistent with the observed lack of product inhibition during dimerization catalysis. Similarly, butoxide precursors to 1-butene (species V, ΔH_{ads} = −52 kJ mol^{-1}) would result in coverages of 0.98–0.99 (1 bar, 243 K). Though this would reflect kinetically detectable coverages which were absent from experimental results, a deviation in enthalpy by +10 kJ mol^{-1} would be sufficient to render site coverages of species V undetectable, in contrast to other Ni sites, described in Section 3.4.

The ethene dimerization route on $(Ni-OH)^+$ centers proposed here (Figure 5) is consistent with experimental observations for Ni/Al-MCM-41 materials[16,17] and with the theoretical assessments presented here. The relevant TS involves concerted interactions with Lewis acid–base pairs in $(Ni-OH)^+$ moiety, which polarizes two bound ethene molecules in opposite directions, thus enabling the electron rearrangements required to form a new C–C bond. Such concerted pathways and the involvement of $(Ni-OH)^+$ as LA–LB site pairs have not been previously considered but represent very active sites that catalyze dimerization turnovers at rates unprecedented for heterogeneous catalysts and at cryogenic temperatures (240–260 K). These pathways are enabled by intrapore liquids that preferentially stabilize the late dimer desorption transition states relative to those that mediate C–C bond formation, thus rendering active sites

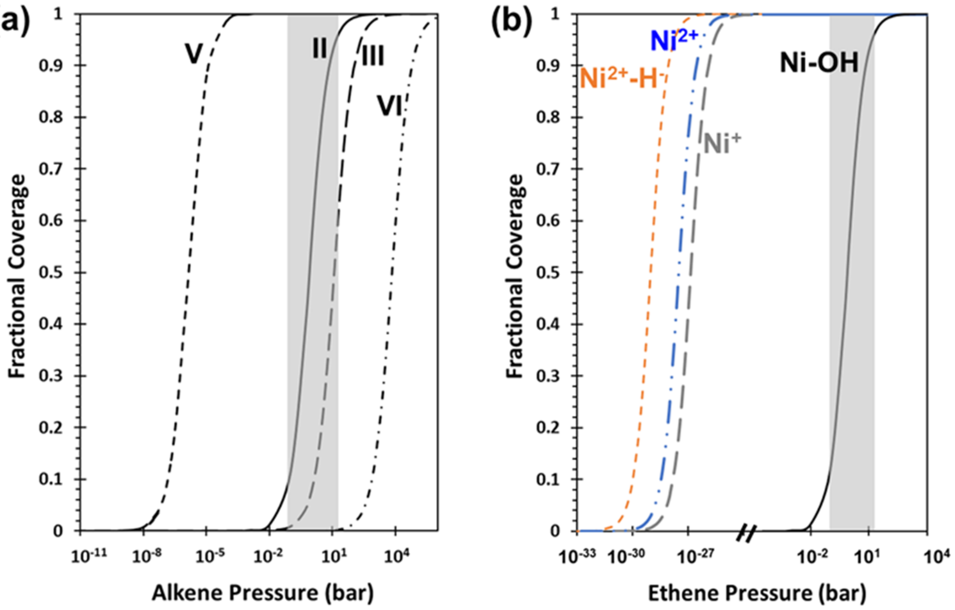

Figure 6. Computed fractional coverages of single species with respect to bare sites for a range of pressures at 243 K for (a) each species in the proposed Lewis acid–base-catalyzed dimerization onto $(\text{Ni–OH})^+$ sites and (b) one ethene adsorbed to $(\text{Ni–OH})^+$ sites (black solid line), Ni^{2+} sites (blue dash-dotted line), $Ni^{2+}–H^-$ (orange dotted line), and Ni^+ (gray dashed line). The gray bar represents typical ethene pressures in dimerization catalysis.

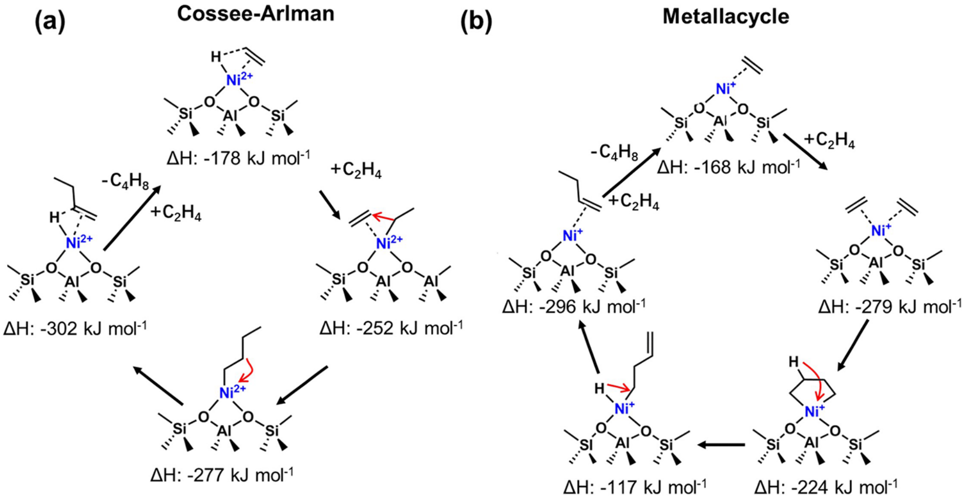

Figure 7. Ethene dimerization catalytic cycles and enthalpies for reaction steps of the (a) Cossee–Arlman pathway on $Ni^{2+}–H$ sites and (b) metallacycle pathway on Ni^+ sites.

stable and free of large oligomers.[16,17] Higher temperatures would selectively increase desorption rates because of their inherent entropy gains (see reaction coordinate diagram at 500 K in Figure S4) but would also preclude the formation of intrapore liquids. As such, extensions of the mechanistic conclusions reported here to higher temperatures or lower pressures (e.g., by microkinetic modeling) would require explicit theoretical treatments of solvation by a dense liquid phase to balance the effects of temperature on free energies of desorption and C–C coupling transition states with those that lead to different extents of pore filling with changes in temperature. Reaction conditions that do not lead to intrapore condensation result in rapid deactivation and the loss of selectivity, rendering these catalysts impractical for use at higher temperatures where alternate mechanistic pathways may prevail. These active centers and pathways differ from Cossee–Arlman and metallacycle mechanisms involving Ni^+ and $Ni^{2+}–H^-$ centers, respectively, which require co-catalysts, such as modified methyl aluminoxane,[66] and activators, such as alkyl aluminum[67,68] or boron compounds (e.g., $B(C_6F_5)_3$ or $B(Ph)_3$),[66] for high reactivity.

The next section provides theoretical evidence to show that Cossee–Arlman or metallacycle routes on Ni^+ and $Ni^{2+}–H^-$ centers cannot account for the observed kinetic trends; such pathways and active centers are also inconsistent with the effects of titrants and thermal treatments on reactivity and the observed dependence of Ni content on alkene dimerization turnover rates for ethene, propene, and 1-butene.[16,17]

3.4. Dimerization via Cossee–Arlman ($Ni^{2+}–H^-$) and Metallacylce (Ni^+) Routes.

Second-order alkene dimerization rates[16,17] are consistent with the modest binding energies of ethene on $(\text{Ni–OH})^+$ centers derived from DFT methods on model $(Ni-OH)^+$ sites. Alternate proposals for site structures and mechanisms must consider the requirement that ethene reactants and butene products bind weakly. Active Ni centers in Cossee−Arlman ($Ni^{2+}-H^-$) and metallacycle (Ni^+) mechanisms are created here by placing them at grafting sites in Al-MCM-41. Their binding properties for ethene molecules are assessed using the same DFT methods used above.

The catalytic cycles depicted in Figure 7 represent the accepted elementary steps for these two classical dimerization mechanisms at their respective proposed active Ni structures. Cossee−Arlman pathways proceed via oxidative addition (H-transfer) from $Ni^{2+}-H^-$ to an ethene molecule to form an ethyl fragment that migrates and reacts with an adsorbed ethene molecule to form a bound butyl group that ultimately desorbs as 1-butene. The metallacyle mechanism involves the binding of two ethene molecules to a Ni^+ center to form a nickel−cyclobutane complex that undergoes β-hydride abstraction via reductive elimination steps. These steps ultimately form the bound 1-butene species that subsequently desorb as the dimer product to complete a catalytic turnover.

The DFT-derived enthalpies for the formation of a bound ethene on Ni^+ and $Ni^{2+}-H^-$ centers are −168 and −178 kJ mol^{-1}, respectively; these enthalpies are much more negative than on $(Ni-OH)^+$ centers (−20 kJ mol^{-1}) indicative of stronger binding of ethene species; such strong binding would lead to significant coverages at conditions of dimerization catalysts, and also to very stable, and thus less reactive, bound species. Their DFT-derived free energies of formation are also much more negative than on $(Ni-OH)^+$ centers (−125 and −135 kJ mol^{-1} on Ni^+ and $Ni^{2+}-H^-$, respectively; −0.5 kJ mol^{-1} on $(Ni-OH)^+$). Such free energies would lead Ni^+ and $Ni^{2+}-H^-$ centers to become saturated with ethene at all conditions of interest (Figure 6b), in contradiction with experimental observations that preclude such strong binding. Such saturation coverages of Ni^+ and $Ni^{2+}-H^-$ species are not consistent with the experimental kinetic trends on solid catalysts consisting of Ni^{2+} species grafted on Al-MCM-41.

Moreover, the binding of a second ethene molecule in subsequent steps involved in Cossee−Arlman (Figure 7a) and metallacycle (Figure 7b) routes leads to bimolecular adducts with DFT-derived enthalpies of formation (from two gaseous ethene molecules and a bare Ni site) that are even more negative than for the binding of the first ethene molecule. The Cossee−Arlman mechanism exhibits enthalpies of binding for intermediate steps ranging from −252 kJ mol^{-1} for a bound ethyl fragment with an adsorbed ethene to −302 kJ mol^{-1} for 1-butene adsorbed on $Ni^{2+}-H^-$ (Figure 7a). Adsorbed species are also strongly bound in the metallacycle mechanism (Figure 7b) with enthalpies ranging from −279 kJ mol^{-1} for two adsorbed ethene molecules, −224 kJ mol^{-1} for the nickel−cyclobutane complex, −117 kJ mol^{-1} for the adsorbed butyl, and to −296 kJ mol^{-1} for an adsorbed 1-butene on Ni^+ sites. Such strong negative enthalpies would dictate full site occupation of adsorbed species for $Ni^{2+}-H^-$ and Ni^+. Relative to ethene site occupations for other Ni species shown in Figure 6b, $(Ni-OH)^+$ is the site least likely to exhibit kinetically detectable coverage of ethene at this temperature (243 K) and pressure (0.1−15 bar).

Bare Ni^{2+} centers at aluminosilicate surfaces were also examined as active centers, even though such species would require Al−Al pairs and are not consistent with dimerization rates that decrease at $Ni:H^+$ grafting stoichiometries above unity (expectation of 0.5:1 for Ni^{2+} centers). The DFT-derived adsorption enthalpy for ethene on Ni^{2+} centers is −152 kJ mol^{-1}, a binding strength contradicted by second-order kinetic trends that require Ni centers to remain essentially bare during dimerization reactions (Figure 6b).[16,17] DFT-derived ethene adsorption enthalpies reported previously on Ni^{2+} and Ni^+ species grafted onto AFI zeolite are also negative and similar in magnitude −146 kJ mol^{-1} (Ni^+; ΔG: −82 kJ mol^{-1}, 393 K) and −129 kJ mol^{-1} (Ni^{2+}; ΔG: −59 kJ mol^{-1}, 393 K). An enthalpy of adsorption of −201 kJ mol^{-1} (ΔG: −136 kJ mol^{-1}, 393 K) was computed for a Ni^0 particle; even this strong binding would lead to complete site coverage at the relevant reaction conditions.[49]

The organometallic molecular catalysts that follow these routes require not only $Ni^{2+}-H^-$ and Ni^+ active centers but also co-catalysts and/or activators for practical reaction rates. For instance, $Ni^{2+}-H^-$ species in the Cossee−Arlman route typically use strong hydride donors, such as alkyl aluminum, borane, or borohydride compounds, which are proposed to replace the indigenous ligands on Ni complexes to form hydride or alkyl moieties,[67,69] thus altering the binding and electronic properties of Ni centers. It is plausible, but not mentioned in previous studies, that these systems may form $(Ni-OH)^+$ species if, for example, alkyl aluminum compounds react with H_2O, O_2, or CO_2 present in trace concentrations to form $Al-(OR)_3$ or its hydrolysis/dihydroxylation products and then transfer an OH group as a new ligand at Ni centers.

These comparisons of the binding energy and concomitant coverages of one and two ethene molecules at Ni^+, $Ni^{2+}-H^-$, Ni^{2+}, and $(Ni-OH)^+$ species indicate that only $(Ni-OH)^+$ centers exhibit the weak binding properties required for dimerization rates to retain the second-order dependence on ethene pressure observed experimentally at all reaction conditions (0.1−15 bar, 240−260 K).[16,17] The strong binding of ethene on Ni^+, $Ni^{2+}-H^-$, and Ni^{2+} make such site structures and their associated mechanisms implausible as descriptors of the unprecedented reactivity of Ni-based solid catalysts for dimerization of ethene, propene, and 1-butene.[17] The presence and involvement of $(Ni-OH)^+$ species as active centers are consistent with the theoretical assessments reported here, and also identify a mechanism not considered in the extensive previous literature. This mechanism involves C−C coupling via a kinetically relevant transition state stabilized by concerted interactions with Lewis acid−base pairs, with the O atom acting as the base and the H atom as the acid in polarizing the two ethene molecules bound at $(Ni-OH)^+$ centers.

4. CONCLUSIONS

DFT assessments of Ni catalyst structures in Ni−Al-MCM-41 catalysts for alkene dimerization identify the active Ni species as $(Ni-OH)^+$ and explicate the nature of the site as a Lewis acid−base pair. The relevant reaction pathway for ethene dimerization on $(Ni-OH)^+$ sites we previously proposed[16,17] was, for the first time, revealed as a plausible pathway for ethene dimerization under the reaction conditions examined. A concerted C−C coupling transition state arises from the Lewis acid−base site polarizing the two ethene molecules in opposite directions and reflects TS enthalpies, which correspond well with experimentally derived values. Sites for heterogeneous alkene dimerization in the Cossee−Arlman ($Ni^{2+}-H^-$), metallacyle (Ni^+), and Ni^{2+}-based pathways bind ethene strongly, which is inconsistent with the experimentally undetectable coverages of ethene-derived species during ethene dimerization. Instead of classical Cossee–Arlman or metallacycle pathways, a concerted Lewis acid–base pathway on $(Ni–OH)^+$ sites prevails as the dimerization mechanism on Ni–Al-MCM-41.

■ ASSOCIATED CONTENT

Supporting Information

The Supporting Information is available free of charge at https://pubs.acs.org/doi/10.1021/jacs.2c13487.

Calculation of enthalpies and entropies using statistical mechanics formalisms; supporting computational results; and DFT-optimized atomic coordinates (PDF)

■ AUTHOR INFORMATION

Corresponding Author

Enrique Iglesia – *Department of Chemical and Biomolecular Engineering, University of California at Berkeley, Berkeley, California 94720, United States;* orcid.org/0000-0003-4109-1001; Email: iglesia@berkeley.edu

Author

Nicholas R. Jaegers – *Department of Chemical and Biomolecular Engineering, University of California at Berkeley, Berkeley, California 94720, United States;* orcid.org/0000-0002-9930-7672

Complete contact information is available at: https://pubs.acs.org/10.1021/jacs.2c13487

Notes

The authors declare no competing financial interest.

■ ACKNOWLEDGMENTS

This work used the Extreme Science and Engineering Discovery Environment (XSEDE), which is supported by National Science Foundation grant number ACI-1548562 under allocation CHE200114. The authors acknowledge the Texas Advanced Computing Center (TACC) at The University of Texas at Austin for providing high-performance computing resources used in some of the calculations reported. They also acknowledge Dr. Shuai Wang for some of the initial calculations, Dr. Wenshuo Hu for technical discussions and a careful review of this manuscript, and Dr. Iker Agirrezabal-Telleria for technical discussions, previously published experimental evidence, and significant foundational mechanistic insights.

■ ADDITIONAL NOTE

[a] Experimentally determined values use Ni exchange stoichiometries below unity and that each Ni exchanged up to stoichiometric unity with the MCM-41 Al sites is active for dimerization catalysis.

■ REFERENCES

(1) Suttil, J. A.; McGuinness, D. S. Mechanism of Ethylene Dimerization Catalyzed by Ti(or ′)(4)/Alr3. *Organometallics* **2012**, *31*, 7004–7010.

(2) McGuinness, D. S. Olefin Oligomerization Via Metallacycles: Dimerization, Trimerization, Tetramerization, and Beyond. *Chem. Rev.* **2011**, *111*, 2321–2341.

(3) Ghambarian, M.; Ghashghaee, M.; Azizi, Z.; Balar, M. Structural Diversity of Metallacycle Intermediates for Ethylene Dimerization on Heterogeneous Nimcm-41 Catalyst: A Quantum Chemical Perspective. *Struct. Chem.* **2019**, *30*, 137–150.

(4) Metzger, E. D.; Comito, R. J.; Wu, Z. W.; Zhang, G. H.; Dubey, R. C.; Xu, W.; Miller, J. T.; Dinca, M. Highly Selective Heterogeneous Ethylene Dimerization with a Scalable and Chemically Robust Mof Catalyst. *ACS Sustainable Chem. Eng.* **2019**, *7*, 6654–6661.

(5) Metzger, E. D.; Brozek, C. K.; Comito, R. J.; Dinca, M. Selective Dimerization of Ethylene to 1-Butene with a Porous Catalyst. *ACS Cent. Sci.* **2016**, *2*, 148–161.

(6) Finiels, A.; Fajula, F.; Hulea, V. Nickel-Based Solid Catalysts for Ethylene Oligomerization - a Review. *Catal. Sci. Technol.* **2014**, *4*, 2412–2426.

(7) Joshi, R.; Saxena, A.; Gounder, R. Mechanistic Insights into Alkene Chain Growth Reactions Catalyzed by Nickel Active Sites on Ordered Microporous and Mesoporous Supports. *Catal. Sci. Technol.* **2020**, *10*, 7101–7123.

(8) Tanaka, M.; Itadani, A.; Kuroda, Y.; Iwamoto, M. Effect of Pore Size and Nickel Content of Ni-Mcm-41 on Catalytic Activity for Ethene Dimerization and Local Structures of Nickel Ions. *J. Phys. Chem. C* **2012**, *116*, 5664–5672.

(9) Tanaka, M.; Kuroda, Y.; Iwamoto, M. Reply to "Comment on 'Effect of Pore Size and Nickel Content of Ni-Mcm-41 on Catalytic Activity for Ethene Dimerization and Local Structures of Nickel Ions'. *J. Phys. Chem. C* **2012**, *116*, 22649–22651.

(10) Lapidus, A. L.; Isakov, Y. I.; Slinkin, A. A.; Avetisya, R. V.; Minachev, K. M.; Eidus, Y. T. Nickel Forms - Components of Nickel-Aluminium Silicate Catalysts of Ethylene Dimerization. *Izv. Akad. Nauk SSSR, Ser. Khim.* **1971**, 1797–1801.

(11) Martínez, A.; Arribas, M. A.; Concepcion, P.; Moussa, S. New Bifunctional Ni-H-Beta Catalysts for the Heterogeneous Oligomerization of Ethylene. *Appl. Catal., A* **2013**, *467*, 509–518.

(12) Cai, T. X.; Cao, D. X.; Song, Z. Y.; Li, L. H. Catalytic Behavior of Niso4/Gamma-Al2o3 for Ethene Dimerization. *Appl. Catal., A* **1993**, *95*, L1–L7.

(13) Davydov, A. A.; Kantcheva, M.; Chepotko, M. L. Ftir Spectroscopic Study on Nickel(Ii)-Exchanged Sulfated Alumina: Nature of the Active Sites in the Catalytic Oligomerization of Ethene. *Catal. Lett.* **2002**, *83*, 97–108.

(14) Saxena, A.; Joshi, R.; Seemakurthi, R. R.; Koninckx, E.; Broadbelt, L. J.; Greeley, J.; Gounder, R. Effect of Nickel Active Site Density on the Deactivation of Ni-Beta Zeolite Catalysts During Ethene Dimerization. *ACS Eng. Au* **2022**, *2*, 12–16.

(15) Brogaard, R. Y.; Komurcu, M.; Dyballa, M. M.; Botan, A.; Van Speybroeck, V.; Olsbye, U.; De Wispelaere, K. Ethene Dimerization on Zeolite-Hosted Ni Ions: Reversible Mobilization of the Active Site. *ACS Catal.* **2019**, *9*, 5645–5650.

(16) Agirrezabal-Telleria, I.; Iglesia, E. Stabilization of Active, Selective, and Regenerable Ni-Based Dimerization Catalysts by Condensation of Ethene Withinordered Mesopores. *J. Catal.* **2017**, *352*, 505–514.

(17) Agirrezabal-Telleria, I.; Iglesia, E. Mechanistic Insights and Consequences of Intrapore Liquids in Ethene, Propene, and Butene Dimerization on Isolated Ni2+ Sites Grafted within Aluminosilicate Mesopores. *J. Catal.* **2020**, *389*, 690–705.

(18) Kresse, G.; Furthmuller, J. Efficient Iterative Schemes for Ab Initio Total-Energy Calculations Using a Plane-Wave Basis Set. *Phys. Rev. B: Condens. Matter Mater. Phys.* **1996**, *54*, 11169–11186.

(19) Towns, J.; Cockerill, T.; Dahan, M.; et al. XSEDE: Accelerating Scientific Discovery. *Comput. Sci. Eng.* **2014**, *16*, 62–74.

(20) Kresse, G.; Joubert, D. From Ultrasoft Pseudopotentials to the Projector Augmented-Wave Method. *Phys. Rev. B: Condens. Matter Mater. Phys.* **1999**, *59*, 1758.

(21) Perdew, J. P.; Burke, K.; Ernzerhof, M. Generalized Gradient Approximation Made Simple. *Phys. Rev. Lett.* **1996**, *77*, 3865–3868.

(22) Grimme, S.; Ehrlich, S.; Goerigk, L. Effect of the Damping Function in Dispersion Corrected Density Functional Theory. *J. Comput. Chem.* **2011**, *32*, 1456–1465.

(23) Monkhorst, H. J.; Pack, J. D. Special Points for Brillouin-Zone Integrations. *Phys. Rev. B: Condens. Matter Mater. Phys.* **1976**, *13*, 5188–5192.

(24) Wang, S.; Iglesia, E. Mechanism of Isobutanal-Isobutene Prins Condensation Reactions on Solid Bronsted Acids. *ACS Catal.* **2016**, *6*, 7664−7684.

(25) Henkelman, G.; Uberuaga, B. P.; Jónsson, H. A Climbing Image Nudged Elastic Band Method for Finding Saddle Points and Minimum Energy Paths. *J. Chem. Phys.* **2000**, *113*, 9901−9904.

(26) Henkelman, G.; Uberuaga, B. P.; Jonsson, H. A Climbing Image Nudged Elastic Band Method for Finding Saddle Points and Minimum Energy Paths. *J. Chem. Phys.* **2000**, *113*, 9901−9904.

(27) Henkelman, G.; Jonsson, H. Improved Tangent Estimate in the Nudged Elastic Band Method for Finding Minimum Energy Paths and Saddle Points. *J. Chem. Phys.* **2000**, *113*, 9978−9985.

(28) Henkelman, G.; Jónsson, H. A Dimer Method for Finding Saddle Points on High Dimensional Potential Surfaces Using Only First Derivatives. *J. Chem. Phys.* **1999**, *111*, 7010−7022.

(29) McQuarrie, D. *Statistical Mechanics*; University Science Books: Sausalito, CA, 2000; pp 222−223.

(30) Sprowl, L. H.; Campbell, C. T.; Árnadóttir, L. Hindered Translator and Hindered Rotor Models for Adsorbates: Partition Functions and Entropies. *J. Phys. Chem. C* **2016**, *120*, 9719−9731.

(31) Deshlahra, P.; Iglesia, E. Methanol Oxidative Dehydrogenation on Oxide Catalysts: Molecular and Dissociative Routes and Hydrogen Addition Energies as Descriptors of Reactivity. *J. Phys. Chem. C* **2014**, *118*, 26115−26129.

(32) Deshlahra, P.; Iglesia, E. Reactivity and Selectivity Descriptors for the Activation of C−H Bonds in Hydrocarbons and Oxygenates on Metal Oxides. *J. Phys. Chem. C* **2016**, *120*, 16741−16760.

(33) Johnson, R. D.*NIST Computational Chemistry Comparison and Benchmark Database*, Nist Standard Reference Database Number 101; NIST, 2022. http://cccbdb.nist.gov/ (accessed 2022-04-04).

(34) Yaws, C. *Yaws Handbook of Thermodynamic Properties*; Gulf Publishing Company, 2007.

(35) Cramer, C. J. *Essentials of Computational Chemistry: Theories and Models*; Wiley, 2005; p 618.

(36) Ugliengo, P.; Sodupe, M.; Musso, F.; Bush, I. J.; Orlando, R.; Dovesi, R. Realistic Models of Hydroxylated Amorphous Silica Surfaces and Mcm-41 Mesoporous Material Simulated by Large-Scale Periodic B3lyp Calculations. *Adv. Mater.* **2008**, *20*, 4579−4583.

(37) Makov, G.; Payne, M. Periodic Boundary Conditions in Ab Initio Calculations. *Phys. Rev. B: Condens. Matter Mater. Phys.* **1995**, *51*, 4014.

(38) Neugebauer, J.; Scheffler, M. Adsorbate-Substrate and Adsorbate-Adsorbate Interactions of Na and K Adlayers on Al (111). *Phys. Rev. B: Condens. Matter Mater. Phys.* **1992**, *46*, 16067.

(39) Makov, G.; Payne, M. C. Periodic Boundary-Conditions in Ab-Initio Calculations. *Phys. Rev. B: Condens. Matter Mater. Phys.* **1995**, *51*, 4014−4022.

(40) Jones, A. J.; Iglesia, E. The Strength of Bronsted Acid Sites in Microporous Aluminosilicates. *ACS Catal.* **2015**, *5*, 5741−5755.

(41) Carr, R. T.; Neurock, M.; Iglesia, E. Catalytic Consequences of Acid Strength in the Conversion of Methanol to Dimethyl Ether. *J. Catal.* **2011**, *278*, 78−93.

(42) Deshlahra, P.; Carr, R. T.; Iglesia, E. Ionic and Covalent Stabilization of Intermediates and Transition States in Catalysis by Solid Acids. *J. Am. Chem. Soc.* **2014**, *136*, 15229−15247.

(43) Moussa, S.; Concepcion, P.; Arribas, M. A.; Martinez, A. Nature of Active Nickel Sites and Initiation Mechanism for Ethylene Oligomerization on Heterogeneous Ni-Beta Catalysts. *ACS Catal.* **2018**, *8*, 3903−3912.

(44) Joshi, R.; Zhang, G. H.; Miller, J. T.; Gounder, R. Evidence for the Coordination-Insertion Mechanism of Ethene Dimerization at Nickel Cations Exchanged onto Beta Molecular Sieves. *ACS Catal.* **2018**, *8*, 11407−11422.

(45) Jaegers, N. R.; Khivantsev, K.; Kovarik, L.; Klas, D. W.; Hu, J. Z.; Wang, Y.; Szanyi, J. Catalytic Activation of Ethylene C−H Bonds on Uniform D8 Ir(I) and Ni(Ii) Cations in Zeolites: Toward Molecular Level Understanding of Ethylene Polymerization on Heterogeneous Catalysts. *Catal. Sci. Technol.* **2019**, *9*, 6570−6576.

(46) Yabushita, M.; Imanishi, Y.; Xiao, T.; Osuga, R.; Nishitoba, T.; Maki, S.; Kanie, K.; Cao, W.; Yokoi, T.; Muramatsu, A. Transcription-Induced Formation of Paired Al Sites in High-Silica Cha-Type Zeolite Framework Using Al-Rich Amorphous Aluminosilicate. *Chem. Commun.* **2021**, *57*, 13301−13304.

(47) Khivantsev, K.; Derewinski, M.; Jaegers, N.; Bogalaienko, D.; Pereira Hernandez, X. I.; Pearce, C.; Wang, Y.; Szanyi, J. *Increasing Al-Pair Abundance in SSZ-13 Zeolite via Zeolite Synthesis in the Presence of Alkaline Earth Metal Hydroxide Produces Hydro-Thermally Stable Co-, Cu- and Pd-SSZ-13 Materials*; ChemRxiv, 2022. DOI: 10.26434/chemrxiv-2022-4hzng-v2 (accessed April 13, 2022).

(48) Xu, J. H.; Wang, R. F.; Zheng, L. R.; Ma, J. G.; Yan, W. J.; Yang, X. F.; Wang, J. Y.; Su, X.; Huang, Y. Q. Unraveling the Real Active Sites of an Amorphous Silica-Alumina-Supported Nickel Catalyst for Highly Efficient Ethylene Oligomerization. *Catal. Sci. Technol.* **2021**, *11*, 1510−1518.

(49) Brogaard, R. Y.; Olsbye, U. Ethene Oligomerization in Ni-Containing Zeolites: Theoretical Discrimination of Reaction Mechanisms. *ACS Catal.* **2016**, *6*, 1205−1214.

(50) Werber, F. X. Polymerization of Olefins on Supported Catalysts. *Adv. Polym. Sci.* **1959**, 180−191.

(51) Sarazen, M. L.; Iglesia, E. Experimental and Theoretical Assessment of the Mechanism of Hydrogen Transfer in Alkane-Alkene Coupling on Solid Acids. *J. Catal.* **2017**, *354*, 287−298.

(52) Tabak, S. A.; Krambeck, F. J.; Garwood, W. E. Conversion of Propylene and Butylene over Zsm-5 Catalyst. *AIChE J.* **1986**, *32*, 1526−1531.

(53) Quann, R. J.; Green, L. A.; Tabak, S. A.; Krambeck, F. J. Chemistry of Olefin Oligomerization over Zsm-5 Catalyst. *Ind. Eng. Chem. Res.* **1988**, *27*, 565−570.

(54) Norton, C. J. Olefin Polymerization over Synthetic Molecular Sieves. *Ind. Eng. Chem. Process Des. Dev.* **1964**, *3*, 230.

(55) Johnson, O. Acidity and Polymerization Activity of Solid Acid Catalysts. *J. Phys. Chem. A* **1955**, *59*, 827−831.

(56) Sarazen, M. L.; Iglesia, E. Effects of Charge, Size, and Shape of Transition States, Bound Intermediates, and Confining Voids in Reactions of Alkenes on Solid Acids. *ChemCatChem* **2018**, *10*, 4028−4037.

(57) Sauer, J.; Schroder, K. P.; Termath, V. Comparing the Acidities of Microporous Aluminosilicate and Silico-Aluminophosphate Catalysts: A Combined Quantum Mechanics-Interatomic Potential Function Study. *Collect. Czech. Chem. Commun.* **1998**, *63*, 1394−1408.

(58) Deshlahra, P.; Iglesia, E. Reactivity Descriptors in Acid Catalysis: Acid Strength, Proton Affinity and Host−Guest Interactions. *Chem. Commun.* **2020**, *56*, 7371−7398.

(59) Arteca, G. A.; Mezey, P. G. Validity of the Hammond Postulate and Constraints on General One-Dimensional Reaction Barriers. *J. Comput. Chem.* **1988**, *9*, 728−744.

(60) Thornton, E. R. A Simple Theory for Predicting Effects of Substituent Changes on Transition-State Geometry. *J. Am. Chem. Soc.* **1967**, *89*, 2915.

(61) Thanthiriwatte, K. S.; Hohenstein, E. G.; Burns, L. A.; Sherrill, C. D. Assessment of the Performance of Dft and Dft-D Methods for Describing Distance Dependence of Hydrogen-Bonded Interactions. *J. Chem. Theory Comput.* **2011**, *7*, 88−96.

(62) Smith, D. G. A.; Burns, L. A.; Patkowski, K.; Sherrill, C. D. Revised Damping Parameters for the D3 Dispersion Correction to Density Functional Theory. *J. Phys. Chem. Lett.* **2016**, *7*, 2197−2203.

(63) Qiu, N. X.; Xue, Y.; Guo, Y.; Sun, W. J.; Chu, W. Adsorption of Methane on Carbon Models of Coal Surface Studied by the Density Functional Theory Including Dispersion Correction (Dft-D3). *Comput. Theor. Chem.* **2012**, *992*, 37−47.

(64) Canivet, J.; Aguado, S.; Schuurman, Y.; Farrusseng, D. Mof-Supported Selective Ethylene Dimerization Single-Site Catalysts through One-Pot Postsynthetic Modification. *J. Am. Chem. Soc.* **2013**, *135*, 4195−4198.

(65) Andrei, R. D.; Popa, M. L.; Fajula, F.; Hulea, V. Heterogeneous Oligomerization of Ethylene over Highly Active and Stable Ni-Alsba-15 Mesoporous Catalysts. *J. Catal.* **2015**, *323*, 76−84.
(66) Ittel, S. D.; Johnson, L. K.; Brookhart, M. Late-Metal Catalysts for Ethylene Homo- and Copolymerization. *Chem. Rev.* **2000**, *100*, 1169−1203.
(67) Skupinska, J. Oligomerization of Alpha-Olefins to Higher Oligomers. *Chem. Rev.* **1991**, *91*, 613−648.
(68) Britovsek, G. J. P.; Gibson, V. C.; Wass, D. F. The Search for New-Generation Olefin Polymerization Catalysts: Life Beyond Metallocenes. *Angew. Chem., Int, Ed,* **1999**, *38*, 428−447.
(69) Svejda, S. A.; Johnson, L. K.; Brookhart, M. Low-Temperature Spectroscopic Observation of Chain Growth and Migratory Insertion Barriers in (Alpha-Diimine)Ni(Ii) Olefin Polymerization Catalysts. *J. Am. Chem. Soc.* **1999**, *121*, 10634−10635.

https://doi.org/10.1021/jacs.2c13487